Research on a novel imaging bionic polarization navigation sensor for glimmer environment application*

GUAN Le (关乐)**, LI Shi-qi** (李世奇)**, LIU Sheng** (刘胜)**, and CHU Jin-kui** (褚金奎)**

Key Laboratory for Precision and Nano, Traditional Machining Technology of Ministry of Education, Key Laboratory for Micro/Nano Technology and System of Liaoning Province, Dalian University of Technology, Dalian 116024, China

(Received 10 January 2018; Revised 14 March 2018)

Polarization navigation system is a hotspot in the field of bionic navigation. Compared with point source polarized light navigation sensor, the polarization information acquisition method based on image sensor and imaging technology has better robustness, and it can obtain more polarization information. In this paper, an embedded imaging polarization sensor for glimmer environment application is designed and developed. The multi-channel video processing technology of TMS320DM642 is used to capture the polarization information of charge coupled device (CCD) camera with three channels. The images are processed by digital signal processer (DSP) in real time, and the angle of polarization (AOP) image is calculated simultaneously with an acquisition and calculation speed of 10 frame per second. Sensor can obtain absolute rotation angle, and the AOP image can be displayed on liquid crystal display (LCD). It provides an effective experimental platform for the research of imaging polarization mode navigation device based on embedded system.

Document code: A **Article ID:** 1673-1905(2018)04-0257-5

DOI https://doi.org/10.1007/s11801-018-8010-4

People have found that skylight has a stable polarization distribution with the change of sun position[1,2]. And a variety of insects can use their compound eye to identify the polarized information in the sky. The visual nervous system in desert ants is extremely sensitive to the direction of skylight polarization, which can be applied to navigation and positioning. Each of the neural rods on the retina of the desert ants is made up of two single-direction photoreceptors crossing each other vertically, and it is sensitive to polarized light in the only direction. The neural stem array responds to different polarization direction $\boldsymbol{E}$-vectors and forms a polarization sensitive compass, and it will produce different excitation responses when the direction of the body axis changes. Finally, the polarization-sensitive neurons (POL neurons) solve and decode the polarization information to achieve navigation and positioning[3].

Accordingly, the domestic and foreign scholars have designed the polarization navigation sensor imitated the bionic compound eyes, which broke the limitation of the existing navigation foundation and become the research hotspot of the new bionic navigation technology. Lambrinos[4] designed a multichannel polarization detection device by imitating the sand ants and realized the navigation of a mobile robot. Chu[5] designed a six-channel polarization sensor, which consists of a photodiode, a signal amplifier and a processor, and the metallic gratings polarizer is used. Chahl[6] designed a polarization sensor by imitating dragonfly and realized the measurement of course angle of unmanned aerial vehicle. This kind of polarization sensor is based on the single point measurement method. It measures the angle of polarization (AOP) of one point skylight by simulating the biological mechanism of insect POL neurons, and it can achieve real-time measurement[8-11]. With the improvement of the requirements for measurement accuracy, scholars have developed imaging polarization sensors based on detection system for skylight polarization pattern, so the dimension of measurement changes from one dimension to two dimensions. Hu[12,13] developed an imaging polarization navigation sensor, which uses four-channel charge coupled device (CCD) to capture images, and calculates the skylight polarization pattern on computer. Takashi Tokuda[14] integrated a multi-directional polarizer on a CMOS image sensor, which dramatically reduced the size of the polarization imaging system. This kind of polarization sensor is based on polarization imaging technology, so it has more polarization

* This work has been supported by the National Natural Science Foundation of China (Nos.51675076 and 51505062), the Science Fund for Creative Research Groups of NSFC (No.51621064), and the Basic Scientific Research Fees for Central Universities (Nos.DUT17GF109 and DUT16TD20).

** E-mail: chujk@dlut.edu.cn

information. Due to the large amount of data with a low real time, it usually runs on the host computer[15-17].

It has been found that the degree of polarization (DOP) and AOP are not affected by the light intensity, so a stable polarization distribution pattern can still be detected in twilight and moonlight[18,19]. Currently, research on polarization sensor for glimmer environment application is not sufficient. Considering the applicability of glimmer, imaging polarization sensor is superior to single point sensor.

This paper describes the design of imaging polarization navigation sensor. The low illumination CCD is used to capture image, and AOP can be obtained in real time by embedded device. This system has the characteristics of miniaturization, real-time performance and strong ability to expand, so it can apply to polarization navigation for glimmer environment applications.

The polarization state of the point light source can be represented by the Stokes vector $\boldsymbol{S}_{\text{in}}=[I, Q, U, V]^{\text{T}}$, where I is the total light intensity, Q and U represent the linearly polarized light intensity in ±45° directions, and V is circularly polarized light intensity. The circularly polarized light in the atmospheric polarization field is weak, so it is negligible in the calculation. The Stokes vector $\boldsymbol{S}_{\text{in}}$ of incident light can be changed when it passes through the polarizer, and the relationship satisfies the Miller matrix, which is shown as

$$\boldsymbol{M}_{\text{mueller}}(\varphi)=\frac{1}{2}\begin{bmatrix}1 & \cos 2\varphi & \sin 2\varphi & 0\\ \cos 2\varphi & \cos^2 2\varphi & \sin 2\varphi\cos 2\varphi & 0\\ \sin 2\varphi & \sin 2\varphi\cos 2\varphi & \sin^2 2\varphi & 0\\ 0 & 0 & 0 & 0\end{bmatrix}, \tag{1}$$

$$\boldsymbol{S}_{\text{out}}=[I(\varphi),\ Q(\varphi),\ U(\varphi)]^{\text{T}}=\boldsymbol{M}_{\text{mueller}}(\varphi)\cdot\boldsymbol{S}_{\text{in}}, \tag{2}$$

where φ is the angle between transmission axis of the polarizer and reference axis.

The AOP c of incident light can be obtained when it passes through three more polarizers in different φ,which is shown as

$$x=\frac{1}{2}\tan^{-1}\left(\frac{u}{Q}\right). \tag{3}$$

The sensor system consists of CCD, linear polarizing filter, optical zoom lens, digital signal processor (DSP), analog-to-digital (A/D) video decoder, inter-integrated circuit (IIC) bus multiplexer, digital-to-analog (D/A) video encoder and liquid crystal display (LCD). The specific composition structure of sensor system is shown in Fig.1.

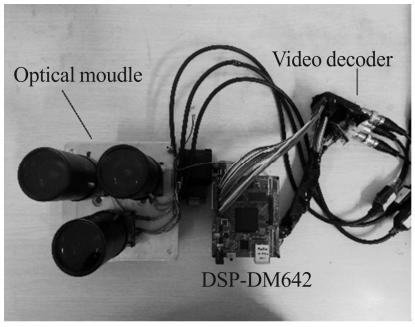

Fig.1 Composition structure of sensor

According to functions, the sensor system is divided into optical processing module, digital signal processing module, debugging module and output module. The optical processing module completes the collection of external light and the capture of image. The digital signal processing module completes the preprocessing of the image, filtering and calculations. The output module outputs the angle through the network port and converts the AOP image into an analog video signal, and displays the skylight polarization pattern (AOP image) on LCD. The overall framework of the sensor is shown in Fig.2.

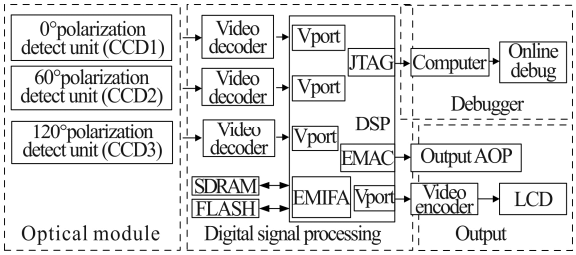

Fig.2 The overall framework of the sensor

The optical imaging module consists of three CCD cameras, three-piece zoom lens and a linear polarizer. Camera captures images of the zenith region. The linear polarizing filter is be installed in front of the lens, which are 0°, 60° and 120° relative to the reference axis of sensor. Three-piece zoom lens with F=1.8 and focal length of 5—100 mm converges the light on the CCD image sensor. The optical imaging module is shown in Fig.3.

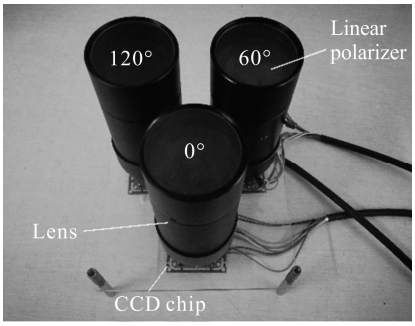

Fig.3 Optical imaging module

CCD has better photosensitivity than CMOS, so the CCD has good nighttime applicability. The CCD camera we used is a combination of Sony 673 CCD sensor with pixels of 610 000, minimum illumination of 0.01Lux/F1.2 and signal-to-noise ratio (SNR)≥48 dB and a 4140Effio image processing chip. Output signal format of CCD is analog signal (component video) with 25 Hz PAL standard. The chip of A/D video decoder is TVP5150, which has the characteristics of simple configuration, low power consumption and small package, and can digitize component video as digital signals

(standard: ITU-R BT.656, accuracy: 8 Bits). There is an easy way to configure internal registers and device addresses for TVP5150 by IIC bus.

The DSP we used is DM642 board, and core chip is TMS320DM642 produced by Texas Instruments. This chip is 32-bit fixed-point DSP with frequency of 600 MHz, and its peripheral integrated three-channel video ports can be seamlessly connected with the video encoder. So it usually can be used to the multi-channel videos processing and high-speed computing in real time. VP0 A/B channels of video port in DM642 are connected with two video decoders TVP5150, respectively. VP1 is connected with a TVP5150. The DSP synchronously receives the video data sent by TVP5150 and the direct memory access (DMA) stores the video data in video buffer in data memory. VP2 is connected with D/A video encoder SAA7105 which can display the AOP image on LCD. Because TVP5150 has only two addresses, the IIC multiplexing chip PCA9548A is selected to communicate with three TVP5150. Firstly, DM642 reads the hardware address of the PCA9548A through the IIC bus and writes the chip select data into the internal registers. The PCA9548A connects the IIC bus of the DM642 to each TVP5150 to implement multiple hardware communication. The hardware system diagram is shown in Fig.4.

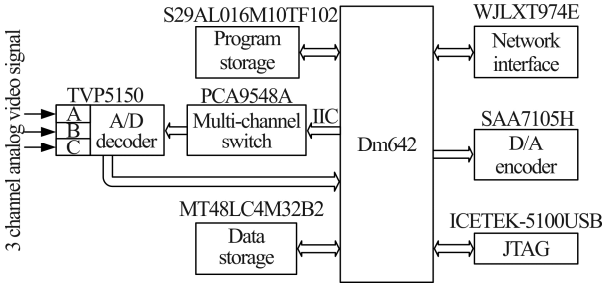

Fig.4 Hardware system diagram

Each image frame has 576 pixel×720 pixel (810 KB) that are stored in data storage and the data format is Y-C_b-C_r (4:2:2), where Y is the luminance signal, C_b is the blue component, and C_r is the red component. Since the luminance Y and the light intensity I are both linear, the calculation of the AOP χ can be considered as the calculation of the luminance. The Stokes vector of the incident light (x, y) on CCD image can be obtained by Eqs.(1) and (2), and when φ=0°, 60° and 120°, it is shown as

$$\begin{bmatrix} I(x,y) \\ Q(x,y) \\ U(x,y) \end{bmatrix} = \frac{2}{3}\begin{bmatrix} 1 & 1 & 1 \\ 2 & -1 & -1 \\ 0 & \sqrt{3} & -\sqrt{3} \end{bmatrix}\begin{bmatrix} Y_{0^\circ}(x,y) \\ Y_{60^\circ}(x,y) \\ Y_{120^\circ}(x,y) \end{bmatrix}. \quad (4)$$

So $\chi(x, y)$ satisfy the following relationship as

$$\chi(x,y) = \frac{1}{2}\tan^{-1}\left(\sqrt{3}\times\frac{Y_{60^\circ}(x,y)-Y_{120^\circ}(x,y)}{2Y_{0^\circ}(x,y)-Y_{60^\circ}(x,y)-Y_{120^\circ}(x,y)}\right). \quad (5)$$

Because CCD will produce photon noise and stochastic noise in glimmer environment. Firstly, we use the median filter to reduce noise, and average the $\chi(x, y)$ on the center (($m-i$)×($n-j$)) of image, so the sensor output is χ_{avg}, which is expressed as

$$\chi_{avg} = \frac{\sum_{x=i}^{m}\sum_{y=j}^{n}\chi(x,y)}{(m-i)(n-j)}. \quad (6)$$

In the skylight polarization pattern, AOP is the angle between E-vector and direction of observation. But $\chi(x, y)$ is the angle between E-vector and the reference axis of image as shown in Fig.5. Coordinate transformation is necessary for the skylight polarization pattern, the post-transformation AOP $\chi_{sky}(x, y)$ satisfies the following relationship that

$$\chi_{sky}(x, y)=\chi(x, y)+\theta. \quad (7)$$

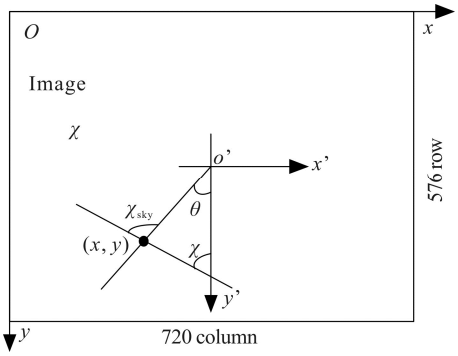

Fig.5 Coordinate transformation diagram

The software design of the sensor system mainly includes the initialization of the DSP chip, the capture of the photograph, the calculation and filtering of the AOP, the output of the average AOP-χ_{avg} and the AOP image-χ_{sky}. The internal initialization of the DSP chip is first completed after being powered on, which includes clock and memory initialization, global variable initialization, interrupt vector table initialization and IIC bus initialization. The program flow chart is shown in Fig.6.

The output of angle χ_{avg} can be obtained from each pixel when the incident light source is single directional linear polarized light. We do the static test of sensor about χ_{avg} in the room. The optical lens with a short focal length (f=30 mm) is used to capture the stable linear polarized light from the integrating sphere, and the sensor rotates every 10° by the precision turntable, as shown in Fig.7. There are 200 pixel×200 pixel in the center of AOP image which were selected for the mean processing, the output of the sensor χ_{avg} under the single directional linear polarized light is shown in Fig.8, and the output range is −90°—90°. It is proved that the sensor can be used in single directional polarization light source with a good linearity, and the angle error is ±2°.

We use the imaging polarization sensor to capture real sky on the roof of School of Mechanical Engineering, Dalian University of Technology, where solar zenith is 82°73′, and solar azimuth is 257°54′. The parameters of the optical lens are the aperture F1.8 and the focal length

f=100. Photograph with luminance of 65 captured by CCD is shown in Fig.9(a). We save the AOP image (χ_{sky}) with different angles between the reference axis of sensor and Solar Meridian. It is easy to see that there are obvious random noise in 0° AOP image, which is due to the system noise. But Solar Meridian is still easy to be observed, as shown in Fig.9(c). In 90° AOP image, there are volatility data when χ_{sky} is ±90°, and the Solar Meridian is not obvious, as shown in Fig.9(d). When χ_{sky} value is not 0° or ±90°, AOP image has a good quality with low noise and signal fluctuation, and Solar Meridian is obvious. 20° AOP image is shown in Fig.9(b).

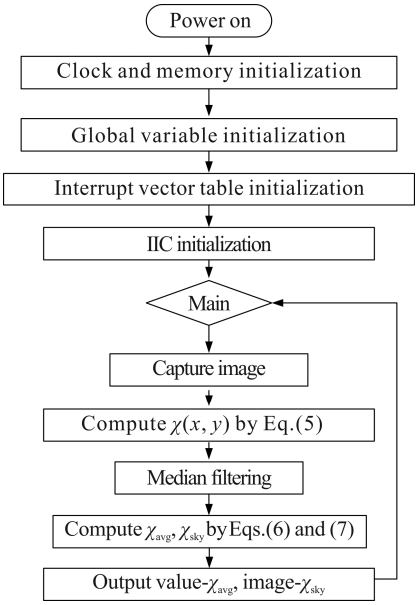

Fig.6 Program flow chart

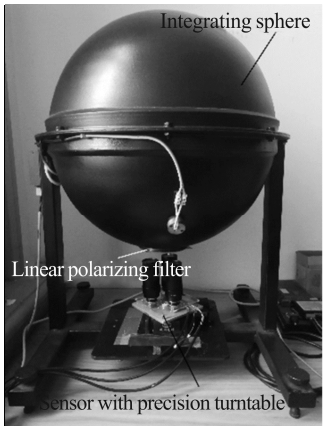

Fig.7 Test under the integrating sphere

In order to test the outdoor output performance of the sensor, we did the test that recording the output of χ_{avg} separately when the angle between reference axis of sensor and geographic North Pole are 0°, 45° and 90°. Look up the solar azimuth by perpetual calendar, and the sensor real orientation can be obtained as shown in Tab.1. It is easy to see that the outdoor accuracy of χ_{avg} is ±5°.

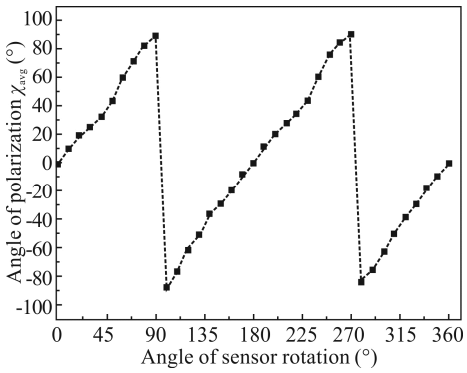

Fig.8 Sensor output under the linear polarized light

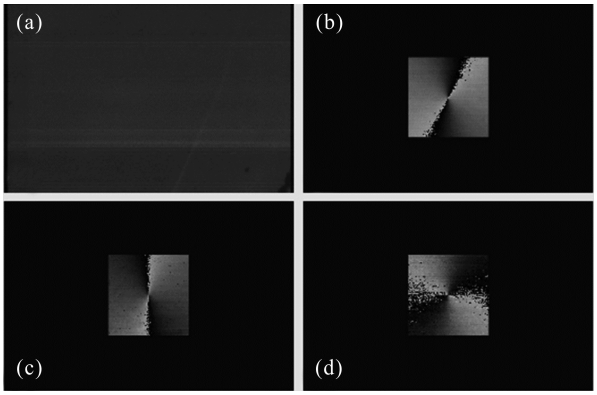

Fig.9 (a) Photograph captured by sensor; (b) 20° AOP image; (c) 0°AOP image; (d) 90°AOP image

Tab.1 Sensor orientation angle test

Sensor orientation	Solar azimuth θ_{AS}	χ_{avg}	$\lvert\theta_{AS}-\chi_{avg}\rvert<\pi/2$
0°	257°56′	10.544 4°	1.52°
0°	257°56′	9.312 9°	2.75°
0°	257°56′	10.844 4°	1.22°
45°	258°48′	53.710 2°	42.51°
45°	258°48′	54.05°	42.85°
45°	258°48′	53.855 6°	42.66°
90°	259°36′	75.192 5°	85.59°
90°	259°36′	77.687 1°	88.09°
90°	259°36′	75.810 5°	86.21°

In this paper, a novel polarization sensor based on embedded system is designed. From the actual capture of the sky in the outdoor experiment, it can be proved that this imaging polarization navigation sensor can obtain more comprehensive AOP information and represent the skylight polarization pattern of the zenith region with a higher robustness. The sensor based on the embedded system can detect the polarization information of the zenith region with a certain real time. Currently, the sensor can calculate 10 frames AOP image in 1 s. This method has the characteristics of small size and modularity compared with the way of calculating by computer. The way to optimize the polarization image captured and how to obtain the Solar Meridian features of AOP image

accurately are the main work in the future. Meanwhile, signal noise is also an important factor affecting the output accuracy of the sensor. Specifically, the fluctuation of the output angle is obvious when the sensor is in steady state, it is steady-state error, which can be compensated by image preprocessing. This is also an important work in later research.

References

[1] Hulst H C, Light Scattering By Small Particle, New York: Wiley, 119 (1957).

[2] Strutt H J W, Philosophical Magazine **41**, 274 (1871).

[3] Pomozi I, Horvath G and Wehner R, Journal of Experimental Biology **204**, 2933 (2001).

[4] Chu J K and Zhao K C, Nanoelectronic Device and Technology **42**, 541 (2005). (in Chinese)

[5] Lambrinos D, Kobayashi H, Pfeifer R, Maris M and Labhart T, Adaptive Behavior **6**, 131 (1997).

[6] Zhang R, Chu Jin-kui, Liu Z and Wang Yin-long, Journal of Micro/Nanolithography, MEMS and MOEMS **15**, 034501 (2016).

[7] Chahl J and Mizutani A, IEEE Sensor Journal **12**, 289 (2012).

[8] Yan L, Guan Gui-xia, Chen Jia-bin, Wu Tai-xia and Shao Xuan, Acta Scientiarum Naturalium Universitatis Pekinensis **45**, 616 (2009). (in Chinese)

[9] Xian Zhi-wen, Hu Xiao-ping, Lian Jun-xiang, Zhang Li-lian, Cao Ju-liang, Wang Yu-jie and Ma Tao, Sensors **14**, 17068 (2014).

[10] Zhang Shuai, Liang Hua-wei, Zhu Hui, Wang Dao-bin and Yu Biao, A Camera-Based Real-Time Polarization Sensor and its Application to Mobile Robot Navigation, IEEE International Conference on Robotics and Biomimetics, 271 (2014).

[11] Wang Yin-long, Chu Jin-kui, Zhang Ran, Wang Lu and Wang Zhi-wen, Science Report **5**, 9725 (2015).

[12] Fan Chen, Hu Xiao-ping, Lian Jun-xiang, Zhang Li-lian and He Xiao-feng, IEEE Sensors Journal **16**, 3640 (2016).

[13] Wang Yu-jie, Hu Xiao-ping, Lian Jun-xiang, Zhang Li-lian, He Xiao-feng and Fan Chen, Journal of Shanghai Jiao Tong University (Science) **22**, 55 (2017).

[14] Takashi T, Hirofumi Y, Kiyotaka S, and Jun O, IEEE International Symposium on Circuits & Systems **3**, 313 (2009).

[15] Li Bin, Guan Le, Liu Qi and Chu Jin-kui, Transducer and Microsystem Technologies **33**, 69 (2014). (in Chinese)

[16] Zhou Jun, Yang Zhong-guang and Huang He, Optik - International Journal for Light and Electron Optics **154**, 100 (2018).

[17] Liang Jian-qi, Yan Hao and Tang Jun, Science Technology and Engineering **17**, 52 (2017). (in Chinese)

[18] Gál J, Horváth G, Barta A and Wehner R, Journal of Geophysical Research: Atmospheres **106**, 22647 (2001).

[19] Cui Yan, Gao Qi-sheng, Chu Jin-kui and Chen Chen, Optics and Precision Engineering **21**, 34 (2013). (in Chinese)